Some laboratory experiments on Rossby waves in a rotating annulus

By ALAN IBBETSON, *Woods Hole Oceanographic Institution*,[1] *and* NORMAN PHILLIPS, *Massachusetts Institute of Technology*

(Manuscript received September 13, 1965)

ABSTRACT

Rossby waves were generated by a slowly oscillating paddle in a rotating annulus of water. The variation with frequency of the real part of the wave number is very satisfactory, but the experiments give only order-of-magnitude agreement between the observed damping with distance from the source and a theoretical estimate which ignores sidewall boundary layers. Behavior of the waves in a closed basin formed by placing a barrier wall across the annulus 60 degrees up-rotation from the wave source agrees qualitatively with theoretical expectation in that at low frequencies the radial motion is concentrated in the region near the reflecting barrier. This effect is a simple generalization of Stommel's original concept of the westward intensification of steady currents and appears to be present in the oceans.

1. Introduction

The tendency toward a concentration of strong currents in the western part of the oceans is well known and was first explained by Stommel (1948) in a steady-state model as a combination of two effects—friction and the latitudinal variation of the Coriolis parameter. In this paper we present some experimental illustrations of this principle for oscillatory motions. The experiments were done with a rotating annulus of water whose depth increased outward with distance from the rotation axis giving rise to an effect similar to the variation of the Coriolis parameter on the earth. A slowly oscillating paddle with a stationary vertical axis generated the waves.

The oscillatory motions in the experiments are an example of "oscillations of the second class" or *Rossby waves*. The verification with these experiments of the wavelength-frequency relation has already been reported (Phillips, 1965; hereafter referred to as ERW).

2. Apparatus and cxperimental techniques

The experiments were carried out using the rotating table two meters in diameter constructed as a permanent facility at the Woods Hole Oceanographic Institution by Dr. Alan J. Faller.

The table consists of a waterproofed circular plywood base supported at 18 points on leveling screws which are rigidly attached to a circular steel framework. The framework is supported at its center on a flange locked to a stainless steel shaft mounted in bearings, on which the table rotates. The bearings are supported in a steel tripod which is equipped with leveling screws at the lower extremities of its legs.

The rotation axis of the table was aligned with the vertical to within about 4×10^{-5} radian by adjusting the tripod leveling screws and using a precision level having a sensitivity of 4.1×10^{-5} radian per division. Similarly the surface of the rotating table was made flat to within ± 1 mm by adjusting the table leveling screws and using a vertical gauge and cathetometer.

The turntable was rotated at a steady speed, continuously variable up to 1.5 radian $\sec^{-1}$, by a Graham variable speed transmission (model 200W18) driven by a 1 HP 1800 rpm synchronous motor. The rotation of the transmission worm output shaft is transmitted to the rotating table by a Positive Drive belt and pulleys. Fluctuations in the rotation speed of the table having periods of the order of several

[1] Contribution no. 1710 from the Woods Hole Oceanographic Institution.

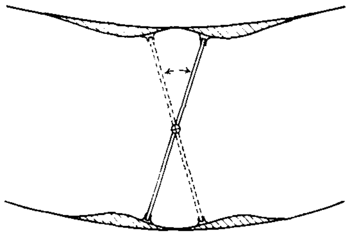

FIG. 1. Overhead plan of oscillating plate used as the wave source.

minutes, and arising from supply voltage and frequency variations, are estimated to be about ± 0.1 per cent of the rotation speed; fluctuations having frequencies of the order of the table rotation frequency, and arising from mechanical inaccuracies in the transmission, are larger (probably ± 0.3 per cent).

The annulus in which the wave motion was generated was constructed by placing a circular Plexiglas cylinder of radius 72.4 ± 0.5 cm inside a second Plexiglas cylinder of radius 102.0 ± 0.5 cm. Both cylinders were 20 cm high, were open at the top, and were closed at the bottom with flat sheets of Plexiglas. The annulus was covered during each experiment with a thin sheet of Plexiglas to prevent the stationary air in the laboratory from exerting a stress on the rotating water surface.

The wave motion was generated mechanically by a vertical plate supported on a vertical axis in the center of the annulus (Fig. 1). This plate ("paddle") was oscillated about its central vertical axis by a reciprocating arm mechanism driven by a variable speed electric motor. The neutral position of the plate was along a radius of the annulus (where it extended completely across the annulus) and the amplitude of the periodic angular displacement from this neutral position could be set at any value up to ± 30 degrees. The period of the oscillating plate was variable from 20 to 100 sec. Fluctuations in the period were less than ± 1 per cent of the value chosen for any single experiment. In order to prevent flow around the edges of the moving plate, its vertical sides and horizontal bottom edge were fitted with "wiper blades" made from thin plastic sheet; these made contact respectively with circular cylindrical sections faired into the sides of the annulus and the bottom of the tank.

The motion of the water in the annulus was made visible by fine particles of aluminium metal floating on its surface. (Because of the small Rossby number in these experiments the flow is very closely two-dimensional i.e. independent of height.) A small quantity of nigrosine dye added to the water improved the visibility of the particles, and a few drops of 'Photo-flo' solution in the water reduced its surface tension and therefore the agglomeration rate of the particles.

Because of the slow fluid motions encountered in these experiments (typically less than 1 cm sec^{-1}), the waves were most conveniently observed photographically. The rotating basin facility included a rotating camera mount, independent of the turntable and about 2.5 meters above it. The axis of rotation of the camera mount was aligned very carefully with that of the rotating basin, and its rotation was synchronized electrically with the rotating basin. Time exposures of the wave motions in the tank were made with a Nikon F 35 mm camera capable of electrical operation remote from the rotating basin. These exposures yielded streak photographs showing the instantaneous velocity field. Cine films of the wave motion were also obtained, using a Bolex 16 mm camera on the rotating camera mount.

All experiments were performed at a fixed rotation rate, $\omega = 1.5$ rad sec^{-1}, and with the same depth of water

$$H = \tfrac{1}{2}\frac{\omega^2 r^2}{g}. \tag{2.1}$$

(H thereby varying approximately from 6 to 12 cm between the inner and outer radii of the annulus.)

3. Open channel experiments

Fig. 2 illustrates the flow pattern produced by the paddle in the absence of any other barrier across the annulus. In ERW it was shown that the frequency of these waves for the depth law (2.1) is given approximately by

$$\sigma = \frac{4\omega s}{s^2 + \lambda^2 + (9)^2}. \tag{3.1}$$

s is the azimuthal angular wave number. λ is equal to

$$\lambda = \pi \div \ln\left(\frac{\text{outer radius}}{\text{inner radius}}\right) \sim \frac{\pi \bar{r}}{D} \sim 9,$$

where $\bar{r}$ is the mean radius and D is the width of the annulus. This large value for λ means that the denominator of (3.1) may be approximated by $s^2 + \lambda^2$.

For a prescribed real value of σ, (3.1) gives two values of s. These are given approximately by

$$\alpha_1 \equiv s_1/\lambda = \mu^{-1}[1 + (1 - \mu^2)^{\frac{1}{2}}],$$

$$\alpha_2 \equiv s_2/\lambda = \mu^{-1}[1 - (1 - \mu^2)^{\frac{1}{2}}], \qquad (3.2)$$

where μ is a non-dimensional frequency:

$$\mu \equiv \sigma/\sigma_{\max}; \quad \sigma_{\max} \equiv 2\omega/\lambda. \qquad (3.3)$$

α_1 and α_2 are real when $\mu < 1$. The short-wave solution, α_1, propagates energy in the direction of rotation (counterclockwise in Fig. 2), while the long-wave solution, α_2, propagates energy opposite to the direction of rotation. This property explains the simultaneous existence of the short and long waves on opposite sides of the paddle in Fig. 2.

The wave trains emitted by the paddle die out before they meet on the opposite side of the annulus, and this damping is presumably due to viscous boundary layers at the bottom, side, and (to a lesser extent) top surfaces of the fluid. The bottom surface has a viscous Ekman layer, of thickness

$$\delta = (\nu/\omega)^{\frac{1}{2}} \sim 1 \text{ mm},$$

where ν is the kinematic viscosity ($\sim 10^{-2}$ cm^2 sec^{-1}). This layer gives rise to a vertical velocity just above it:

$$w = \left(\frac{\nu}{4\omega}\right)^{\frac{1}{2}} \zeta,$$

where ζ is the vertical component of relative vorticity in the interior fluid. A crude estimate of the damping is provided by inserting this effect into the quasi-geostrophic form of the vorticity equation, in the manner of CHARNEY & ELIASSEN (1949), as a lower boundary condition on the inviscid interior flow. The resulting linearized equation is

$$\frac{\partial \zeta}{\partial t} - \left(\frac{2\omega}{H}\frac{dH}{dr}\right)\dot{r} = -\frac{\zeta}{\tau_E},$$

where $\tau_E = H(\nu\omega)^{-\frac{1}{2}}$ is the frictional decay time associated with the Ekman effect, and $\dot{r}$ is the perturbation radial velocity. *If H in τ_E is treated as a constant*, this equation can be solved without having to approximate the cylindrical geometry, by making use of the geostrophic approximation and applying only the non-viscous boundary conditions at the annular walls. If we define

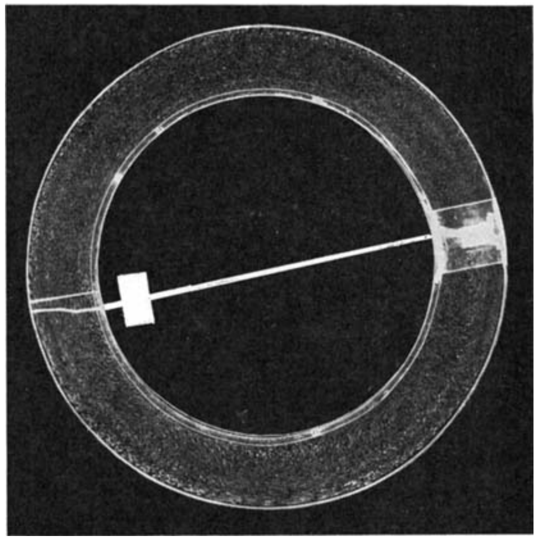

FIG. 2. Full view from above of the wave pattern produced at a paddle period of 25.7 secs ($\mu = 0.737$). The picture is a 5-second time exposure, the camera rotating with the annulus. The paddle is at the right of the photograph, and the annulus is rotating counterclockwise. The theoretical wave lengths for $\mu = 0.737$ are 17.5° and 91° on the down-rotation and up-rotation sides of the paddle, respectively. Paddle amplitude was ± 5 cm.

$$\varkappa = (\tau_E \sigma_{\max})^{-1} = \frac{\lambda}{2\bar{H}}\left(\frac{\nu}{\omega}\right)^{\frac{1}{2}}, \qquad (3.4)$$

the two roots α_1, α_2 corresponding to (3.2) are now given by the (complex) solutions of the quadratic equation

$$\alpha^2 - \frac{2\alpha}{\mu - i\varkappa} + 1 = 0. \qquad (3.5)$$

$\varkappa$ has a value of 0.04 in the experiments.

An important feature of the two roots of (3.5) is that the ratio of the imaginary to the real part of each solution has the same absolute value:

$$\alpha_{1i}/\alpha_{1r} = -\alpha_{2i}/\alpha_{2r} \equiv \Delta/2\pi > 0.$$

In one wave length both wave trains damp by an amount $\exp(-\Delta)$, according to this theory.

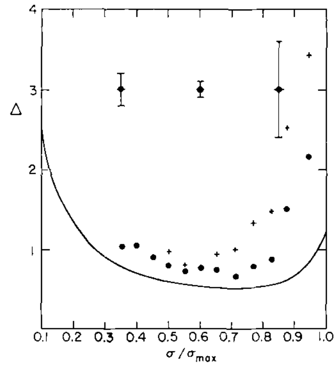

Fig. 3

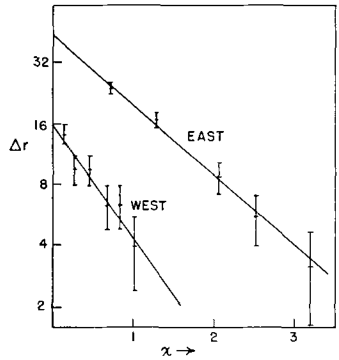

Fig. 4

FIG. 3. Damping rate exponent Δ as a function of the nondimensional frequency $\mu = \sigma/\sigma_{max}$. Crosses and dots are observed values on the up-rotation and down-rotation sides, respectively. The three vertical bars in the upper part of the diagram indicate the variance of the experimental points at three representative frequencies. The curve is the theoretical Ekman damping rate.

FIG. 4. An example of the measured variation with distance from the source of the radial amplitude of particle trajectories at a fixed frequency $\sigma = 0.256$ sec^{-1}. The abscissae is distance from the source in units of the wavelength defined by (3.2). The ordinate is the total amplitude Δr of particle trajectories in mm on a logarithmic scale. *East* and *West* refer to the down-rotation and up-rotation sides of the paddle. Variance is shown by the vertical bars. The straight lines are fitted by eye; their slope is proportional to Δ in Fig. 3.

The minimum value of Δ with respect to μ occurs at $\mu^2 = 0.5 + \varkappa^2$, giving $\Delta_{min} = 4\pi\varkappa = 0.52$. The minimum theoretical amplitude reduction attainable in the experiments is therefore about 60 per cent in one wave length.

Fig. 3 contains a graph of this theoretical value for Δ, together with observed values. The latter were obtained by measuring the radial amplitude of particle trajectories (floating tracers) as a function of distance from the paddle, on time exposure photographs lasting one paddle period (the camera rotating with the annulus). Fig. 4 indicates the accuracy with which the exponential decrement could be determined in this way.

The observed damping rate is uniformly larger than the theoretical Ekman value, a discrepancy which is to be expected from the neglect, in the above theory, of the side-wall boundary layers. Unfortunately, we have not been able to complete a rigorous analysis of these effects. Fig. 3 shows a larger value of the observed damping rate on the up-rotation side compared to that on the down-rotation side. This is qualitatively understandable in that the side-wall viscous boundary layers exist primarily to reduce the azimuthal horizontal velocity there to zero, and the ratio of the azimuthal to the radial component of the horizontal velocity is larger on the up-rotation side, where the wave length is large, than on the down-rotation side.

4. Waves in a closed basin; reflected Rossby waves

As is well known, the presence of meridional barriers in the world ocean introduces profound modifications in the steady large-scale currents. The same effect will also be important for non-steady currents (e.g. Rossby waves), and some aspects of this have been discussed recently by LONGUET-HIGGINS (1964) and by PEDLOSKY (1965). We have performed some simple experiments of this type by introducing a radial barrier across the annulus, 60 degrees "up-rotation" from the paddle. In the theoretical description of this we will retain only the simple Ekman frictional effect.

The linearized differential equation is homogeneous

$$\left(\frac{\partial}{\partial t} + \frac{1}{\tau_E}\right)\nabla^2\psi + \frac{4\omega}{r^2}\frac{\partial\psi}{\partial\theta} = 0,$$

where $\tau_E = \bar{H}(\nu\omega)^{-\frac{1}{2}}$ is the Ekman decay time, and ψ is a stream function. The motion is forced by the paddle (at $\theta = 0$), so that $\psi(r,\theta,t)$ is of the form $\sin(\lambda R)G(\theta)\exp(i\sigma t)$, with $R = \ln$ (outer radius) $-\ln r$. If we define

$$X = (\theta + \theta_0)\lambda,$$

where the paddle is located at $\theta = 0$ and the barrier at $\theta = -\theta_0$, the mathematical problem reduces to the ordinary differential equation

$$(i\mu + \varkappa)\left(\frac{d^2G}{dX^2} - G\right) + 2\frac{dG}{dX} = 0,$$

with the boundary conditions[1]

$$G = 0 \text{ at } X = 0,$$

$$G = 1 \text{ at } X = L = \lambda\theta_0.$$

The solution of this problem is straight forward:

$$\psi = \sin \lambda R \frac{[e^{i(\alpha_1 X + \sigma t)} - e^{i(\alpha_2 X + \sigma t)}]}{e^{i\alpha_1 L} - e^{i\alpha_2 L}}, \qquad (4.1)$$

where α_1 and α_2 are the complex wave numbers defined by (3.5). The theoretical response thus consists simply of the two traveling waves, both with their phase velocity directed to negative X, but with oppositely directed group velocities. The shorter α_1-wave has its maximum amplitude at the barrier ($X = 0$) while the long α_2-wave has its maximum amplitude at the paddle ($X = L$), and the formal solution (4.1) merely adjusts the phase and amplitudes of the two waves to satisfy the two boundary conditions.

Resonance would occur if the denominator in (4.1) were to vanish. With friction present this cannot happen since α_1 and α_2 are complex and unequal. Without friction ($\varkappa = 0$), the denominator would vanish for the frequencies defined by

$$\mu^2 = \mu_m^2 = (1 + m^2\pi^2L^{-2})^{-1}, \qquad (4.2)$$

where $m = 1$, 2 etc. These are the normal modes of oscillation for a frictionless closed rectangular basin (PEDLOSKY, 1965) when, as is justified here, the local time variations in the depth of the fluid are negligible. These free solutions

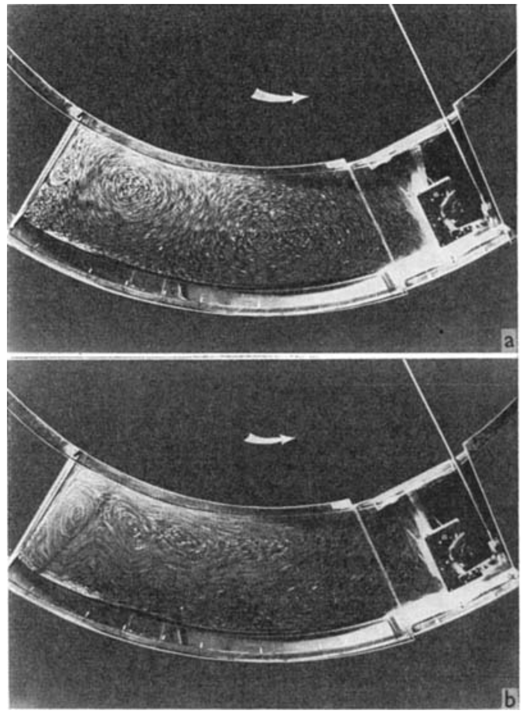

FIG. 5. Wave patterns in closed basin with barrier 60 degrees up-rotation from source. The upper figure (5a) is for a frequency $\mu = 0.85$ and the lower (5b) is for $\mu = 0.37$. These values of μ correspond to $m = 2$ and 7.5 in the formula (4.2). The time exposure is for one-fifth of the paddle period in both cases, and the paddle amplitude in both cases was ± 2.5 cm.

are of the form

$$\psi = \sin \lambda R \sin \frac{m\pi X}{L} \sin (\sigma t + X\mu_m^{-1}), \qquad (4.3)$$

showing that the flow is modulated by a standing pattern of m cells.

With friction present, the response at these values of μ is bounded, but should be larger than at intermediate frequencies. Unfortunately the experimental value of $\varkappa$ (0.04) is large enough that the response is not very peaked at any but the very smallest values of m. The upper picture in Fig. 5 shows an observed flow pattern for the frequency $\mu = \mu_2$. It illustrates very clearly the property of the frictionless free modes (4.3) that the basin is divided into m cells (in this case 2) in the X-direction.

At smaller frequencies, the effect of friction increases, becoming important even before μ

[1] The value of G at $X = L$ is proportional to the product of the paddle amplitude and the paddle frequency, i.e., the forced oscillatory zonal velocity at the paddle. We consider this fixed in the present analysis.

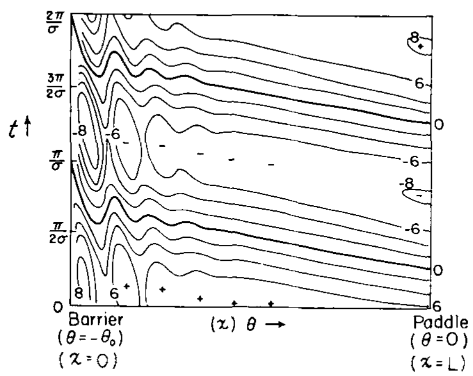

FIG. 6. The theoretical amplitude $\mathrm{Re}\,G(X)\exp(i\sigma t)$ from (4.1) as a function of X and t for $\theta_0=60°$, $\varkappa=0.04$, and $\mu=0.292$ [corresponding to $m=10$ in equation (4.2)].

becomes as small as $\varkappa$. Fig. 6 shows the theoretical variation with X and t of $\mathrm{Re}G(X)\exp i\sigma t$ (in arbitrary units) for the case $\mu=\mu_{10}=0.292\sim 7\varkappa$. There is little tendency for a division into 10 separate cells, since there are only two zero isolines and these extend from left to right instead of from top to bottom in the diagram.

In this frequency range the physical interpretation of the flow pattern is most easily understood in terms of the separate α_1- and α_2-waves, rather than in terms of the free modes of a closed basin. The paddle is sending out the long α_2-wave, whose velocity pattern is mostly in the azimuthal component rather than the radial component. α_2 is small, and this wave reaches the barrier at $X=0$ with practically undiminished amplitude. The boundary condition of no azimuthal velocity at the barrier is then satisfied by the existence of a reflected α_1-wave. At these frequencies both the real and imaginary parts of α_1 are large enough that the amplitude of the reflected α_1-wave becomes very small well before it reaches back to the paddle. The result is a concentration of radial motion in the "western" part of the basin and no resonance. In this frequency range the asymmetry is therefore more pronounced than is indicated by PEDLOSKY (1965). The lower part of Fig. 5 illustrates this type of response in the experiments. The phase velocity of the reflected α_1-wave is of course *toward* the reflecting barrier and this can be readily seen in time-lapse films.

A noticeable feature of the lower part of Fig. 5 is the existence of a steady drift in the azimuthal direction, in one direction in the middle of the annulus and in the other direction near the walls. This appears to be a non-linear effect, arising partly from non-linear advections of vorticity within the fluid and partly from non-linear forcing at the paddle itself. [The forced azimuthal velocity at the paddle, if expanded in powers of the angular amplitude of the paddle, theoretically contains all multiples (including zero) of the basic oscillatory frequency.] These non-linear effects could presumably be reduced relative to the linear response by reducing the paddle amplitude, but the large frictional effect then makes the resulting motions small enough that their detection and measurement becomes difficult.

The type of flow pattern shown in Fig. 5*b* is especially interesting in view of the evidence summarized by M. SWALLOW (1961) that there is considerable meridional eddy motion in the western part of the Atlantic, but relatively little in the eastern part. While conditions in the ocean differ in some important respects from those in the experiments, it would seem likely that an extension of the linear theory to the ocean should be able to explain some aspects of the observed eddy motion.

Acknowledgements

The research was supported in part by the National Science Foundation under contract G-18985 with the Massachusetts Institute of Technology, and in part by the Office of Naval Research under contract No. 2196(00) with the Woods Hole Oceanographic Institution.

REFERENCES

CHARNEY, J., and ELIASSEN, A., 1949, A numerical method for predicting the perturbations of the middle-latitude westerlies. *Tellus*, 1 (2), 38–54.

LONGUET-HIGGINS, M., 1964, Planetary waves on a rotating sphere. *Proc. Roy. Soc.* (*A*), **279**, 446–473.

PEDLOSKY, J., 1965, A study of the time dependent ocean circulation. *J. Atmos. Sci.*, **22**, 267–272.

PHILLIPS, N., 1965, Elementary Rossby waves. *Tellus*, **17**, 295–301.

STOMMEL, H., 1948, The westward intensification of wind-driven ocean currents. *Trans. Amer. Geophys. Union*, **29**, 202–206.

SWALLOW, M., 1961, Measuring deep currents in mid-ocean. *New Scientist*, **9**, 740–743.

НЕКОТОРЫЕ ЛАБОРАТОРНЫЕ ЭКСПЕРИМЕНТЫ ИЗУЧАЮЩИЕ ВОЛНЫ РОССБИ ВО ВРАЩАЮЩЕМСЯ КОЛЬЦЕ

Волны Россби генерировались колебаниями лопасти во вращающемся кольце с водой. Изменения с частотой действительной части волнового числа являются весьма удовлетворительными, но наблюдавшееся затухание волны с расстоянием от источника согласуется только по порядку величины с теретической оценкой, полученной без учета пограничных слоев на боковых стенках. Волны в замкнутом бассейне образовывались при помещении стенки от источника волн под углом 60° по направлению вращения. Радиальное движение в этом случае при низких частотах концентрировалтись в окрестности отражающей стенки, что качественно согласуется с теоретическим предсказанием. Этот эффект является простым обобщением оригинальной концепции Stommel' о интенсификации в западном направлении установившегося потока, что имеет место в океанах.